Nuclear Inst. and Methods in Physics Research B 413 (2017) 1–5

Contents lists available at ScienceDirect

Nuclear Inst. and Methods in Physics Research B

journal homepage: www.elsevier.com/locate/nimb

Electronic stopping power of Ti, V and Cr ions in Ge and Au at 150–500 keV/u energies

R. Linares[a,*], R.V. Ribas[b], J.R.B. Oliveira[b], N.H. Medina[b], H.C. Santos[a,b], C.C. Seabra[a], L. Sigaud[a], E.W. Cybulska[b], W.A. Seale[b], P.R.P. Allegro[b], D.L. Touffen[c], M.A.G. Silveira[d]

[a] Instituto de Física, Universidade Federal Fluminense, Av. Gal. Milton Tavares de Souza, s/n, Niterói, 24230-346, Brazil
[b] Dept. de Física Nuclear, Instituto de Física, Universidade de São Paulo, São Paulo, SP CP 66318, 05314-970, Brazil
[c] Instituto Federal de Educação, Ciência e Tecnologia de São Paulo-IFSP, Guarulhos, SP 07115-000, Brazil
[d] Dept. de Física, Centro Universitário da FEI, S.B.C., SP, Brazil

ARTICLE INFO

Keywords:
Stopping power
Heavy ions
Low energy

ABSTRACT

In this paper new experimental data are presented for the stopping power of Ti, V and Cr ions in Ge and Au, in the 150–500 keV/u energy range. The heavy ions at low energies are produced from the elastic scattering between particles of an energetic primary beam (^{28}Si and ^{16}O) directed onto the primary foil of interest (Ti, V or Cr). Measurements were performed using the transmission method. New experimental data points for the stopping power of Ti in Au were compared with previous measurement. The agreement between these two datasets indicates the consistence of the experimental technique. Our experimental data were also compared to some selected theoretical and semi-empirical methods: i) the Unitary Convolution Approximation, ii) the Binary theory, iii) the SRIM code and iv) the Northcliffe & Schilling tables. The experimental data for Ge foil deviate from the theoretical curves possibly due to the effect of band gap structure of the material in the electronic stopping power. For the systems measured here, we observe that the Binary theory exhibits an overall good agreement. The velocity-proportional dependence of the electronic stopping power in the measured energy range is also discussed.

1. Introduction

There is a growing interest in understanding the details of the complex atomic collisions in the low energy regime. Reliable predictions of the energy loss of charged particles in solids are important for many applied fields [1]. Surface analysis using the Secondary-ion mass spectrometry (SIMS) requires an accurate knowledge of the energy loss of the ion during the sputtering process and depth distributions for heavy-ion implantations are relevant in semiconductor production [2,3]. In nuclear structure experiments, the Doppler shift attenuation method is employed to determine the lifetime of nuclear states [4,5]. In this technique, the stopping power curve is exploited to establish the picosecond timescale for the excited state lifetime measurement. Often these techniques deal with heavy ions slowing down in matter at energies below the Bragg peak.

During the passage of ions through matter, inelastic collisions between the projectile and target atoms are the dominant mechanism of energy loss over a wide range of velocity (i.e. $\upsilon \gg \upsilon_0$, where υ_0 is the Bohr velocity). This mechanism is referred as the electronic stopping power (ESP) since it leads to excitations and ionizations of one or both partner atoms. At energies well above the Bragg peak ($\geqslant$1 MeV/u), the projectile particles move into matter entirely stripped out of their electrons. The ESP in this energy range can be described with few parameters [6,7] and scalings that produce numerical predictions with relatively good accuracy [8,9].

At energies around and below the Bragg peak, the projectile is partially screened by its electrons and, consequently, effects of the dynamical charge state come into play. In the low energy regime, with velocities below 1 atomic unit (a.u.) (equivalent to $\leq$ 25 keV/u), the ESP competes with elastic collisions between the projectile and the target atom. Such a collision depends on the interatomic potential and, within the Born–Oppenheimer approximation, the nuclear stopping is entirely independent of the electronic one. The Lindhard, Scharff and Schiott (LSS) theory was a landmark approach. The LSS theory considers the interaction of a charged particle with a free-electron gas and makes use of the local density approximation to obtain the ESP [10]. According to the LSS theory, the ESP exhibits a velocity-proportional dependence but deviations have been demonstrated for the energy loss of protons in Ge,

* Corresponding author.
E-mail address: rlinares@id.uff.br (R. Linares).

http://dx.doi.org/10.1016/j.nimb.2017.09.030
Received 23 August 2017; Received in revised form 20 September 2017; Accepted 25 September 2017

Cu and Au [11–13]. However, in a nonadiabatic model, Correa et al. [14] have demonstrated a nontrivial connection between the ESP and the nuclear stopping power. State-of-the-art calculations have been performed for protons slowing down in insulators and noble metals using time-dependent density functional (TD-DFT) [15]. Such calculations have managed to describe the expected threshold velocity for Au, due to the role of the d electronic orbit, that causes a significant deviation from the expected velocity-proportional dependence.

The vast majority of recent developments is conducted for proton projectiles in many different media. Few pieces of information are known for heavy ion projectiles, due to both theoretical difficulties that must be circumvented and to the few experimental data available. In this paper, we present new experimental data for the energy loss of Ti, V, Cr ions in Ge and Au targets in the 150–500 keV/u energy range. The stopping power of Ti in Au has been measured previously [16], and it is included here for the sake of comparison with the Ti in Ge target data. Ge and Au were chosen as targets since they exhibit different electronic configurations in the outermost shell, which might affect the ESP for heavy ions. Moreover, accurate knowledge of the stopping power in Au is important in nuclear structure experiments since it is often used as a stopper medium [5,17]. Demands for accurate predictions and the absence of a valid theory for the vast projectile-target-energy phase space make semi-empirical modeling a useful approach. The Northcliffe and Schilling (NS) tables [8] and the SRIM code, based on the Ziegler, Biersack and Littmark procedures [9], are often used for quantitative purposes in applied sciences. Nevertheless, they may contain significant discrepancies between predicted and measured values for high-Z projectiles due to limitations in the extrapolation of the physical description and limited experimental data available for heavy ions. Therefore, we compare our experimental results to the following theoretical and semi-empirical methods: i) the Unitary Convolution Approximation (UCA) [18,19]; ii) the Binary Theory (BT) [20]; iii) NS tables [8] and iv) SRIM code [21].

2. Experimental setup and results

Measurements were carried out at the 8UD-Pelletron Tandem of the University of São Paulo using the elastic scattering technique [22]. The experimental setup is depicted in Fig. 1. Elastic scattering between projectiles, from an energetic beam, and heavy atoms, that compose the thin primary foil, produces heavy ions at low energies. Recoiling atoms, from the primary foil, in kinematic coincidence with the scattered primary particles are the heavy projectile of interest at low velocities. Particles were detected using Si detectors: two of them placed at $\theta_{lab} = 45°$ and 60°, as monitors, and the third one placed on a mobile platform. The monitors, for the detection of the scattered particles of the primary beam, were set about 210 mm from the primary target and with an 8 mm collimator, corresponding to a solid angle $\Omega \sim 1.1$ mrad. The third one, used to detect the recoiling atoms, was mounted 120 mm from the primary foil with a 3 mm collimator ($\Omega \sim 0.5$ mrad). The heavy projectile energy depends on the primary beam species, their energy and the scattering angle. The elastic scattering of either ^{16}O or ^{28}Si at 45°, for instance, produces recoiling particles at different angles. The recoiling angles of the secondary heavy ion beam were found experimentally by determining the maximum of the angular distribution of the recoils, without the secondary foil, in time coincidence with each monitor. Kinematic broadening due to the finite solid angle of the detectors introduce an uncertainty of about 3.5% in the energy of the recoiling particles.

Secondary foils of Ge and Au were mounted on a six-position target holder that moved the targets into and out of the secondary beam. Two positions were left empty for the measurements of the energy of the recoiling particles. The system was placed as close as possible to the detector (less than 5 mm apart) to avoid missing particles due to the angular straggling caused by the secondary target. In this way, we measured the total stopping power, which is composed of the contribution from the electronic and the nuclear stopping. However, for the energies investigated here, the nuclear component is negligible, according to the SRIM code [21]. Henceforth, we refer to our data as ESP.

Energy calibration of the detector for heavy ions is described in detail in Ref. [22]. The experimental data measured without the secondary target in front of the detector were used to build the calibration curve. An example of the energy calibration is shown in Fig. 2. The energy is determined using a Monte Carlo (MC) code that randomly selects the point of elastic scattering within the primary target and calculates the energy losses of the primary beam in the incoming trajectory and the secondary ions in the outgoing trajectory. Stopping powers from [9] are used as inputs to the MC code. Fig. 2 shows a typical calibration curve for the Ti foil with 99 μg/cm^2 thickness. The calibration curve is linear in the enegy range inspected. Nevertheless, we highlight the importance of using thin primary foils to minimize systematic errors in the estimation of the energy loss of heavy atom recoiling in the foil.

The Ti, V and Cr primary targets and Ge and Au secondary targets are self-supported foils produced by vacuum evaporation. Their thicknesses were determined by the energy loss of α particles from a ^{241}Am source. Thickness of the foils are shown in Table 1. Uncertainties in the thickness are mainly from the stopping power of the α particles (estimated in 4%). We evaluate the foil uniformity by measuring the thickness at several points, in both vertical and horizontal directions using a one-millimeter pin–hole cover in front of the ^{241}Am source. The non-uniformity, defined as the standard deviation of the measured

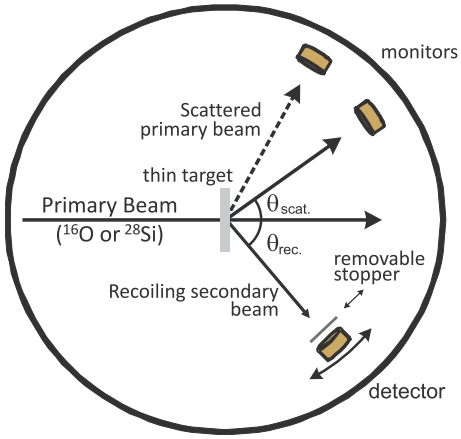

Fig. 1. Experimental setup used for the measurements of the energy loss of Ti, V and Cr in Ge and Au at energies below 500 keV/u. We used ^{16}O and ^{28}Si as primary beams with energies between 32 and 58 MeV, usually with 300 nA beam current.

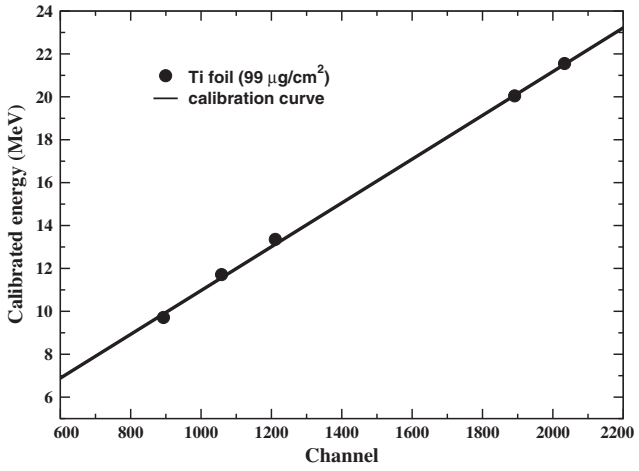

Fig. 2. Energy calibration curve of the detector for Ti ions. See text for details.

Table 1
Thickness Δx (in $\mu g/cm^2$) of Ti, V, Cr, Ge and Au foils. The last column refers to the stopping power for α particles (in MeV/mg/cm^2) adopted to determine the thickness. Two different Ge foils were used. See text for details.

Foil	Δx	dE/dx
Ti	99 ± 6	0.49
V	48 ± 10	0.49
Cr	108 ± 5	0.47
Ge #1	259 ± 11	0.39
Ge #2	108 ± 8	0.39
Au	471 ± 20	0.22

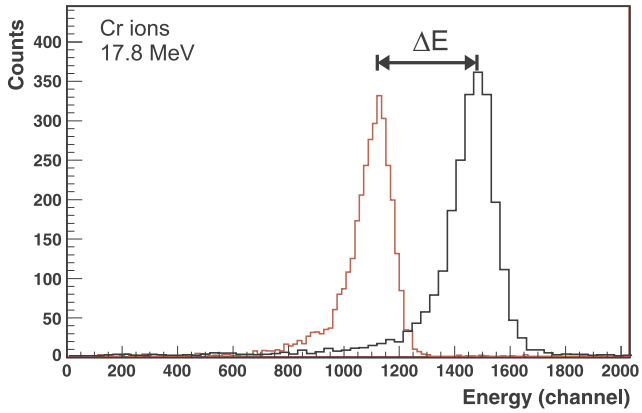

Fig. 3. Typical spectra for Cr ions without (black) and with (red) the Au foil in the beam direction. (For interpretation of the references to colour in this figure legend, the reader is referred to the web version of this article.)

thicknesses for Ge and Au foils was less than 2%.

Typical spectra for 18.7 MeV Cr particles with and without the Au foil are shown in Fig. 3. The differential approach,

$$\frac{dE(\overline{E})}{dx} \simeq \frac{\Delta E}{\Delta x} \quad (1)$$

was applied to compute the experimental stopping power. In this equation, $\Delta E = E_{\text{without}} - E_{\text{with}}$ is the energy loss, where E_{without} and E_{with} are the energies without and with the secondary target of thickness Δx, respectively, placed in front of the detector. The experimental stopping power corresponds to the value at the mean energy $\overline{E} = (E_{\text{without}} + E_{\text{with}})/2$. The differential approach is usually adopted whenever ΔE is a small fraction, less than 15%, of E_{without}. However, considering the smooth behavior of the stopping power curve at energies below the Bragg peak, it is possible to extend it beyond this restriction. Using the TRIM code, we performed simulations of the energy loss of Ti, V, Cr ions in Ge and Au thin foils. The simulation results indicate that the differential approach could be adopted without additional corrections if $\frac{\Delta E}{E_{\text{without}}} \leq 0.3$.

The experimental ESP data for Ti, V, Cr in Ge and Au are presented in Table 2. The Ge foil #1 (see Table 1) was used for the measurements of the energy loss for Ti and Cr while the Ge foil #2 was used for V ions. The electronic stopping power of Ti in Au has been published in Ref. [23] and in Table 2 we present only the new data points. In Fig. 4 the comparison between the previous and the new data for the electronic stopping power of Ti in Au are shown. The agreement is good and indicates the consistency of our experimental technique.

3. Discussions

3.1. The Unitary Convolution Approximation and the Binary theory

The projectile-target interaction is sensitive to the electronic dynamics of both atomic partners in the energy range investigated here.

Table 2
Experimental electronic stopping power of Ti, V and Cr ions in Ge and Au. $\overline{E}$ is the mean energy between the incident and the emergent beam energies. Energies and stopping powers are presented in keV/u and MeV/mg/cm^2, respectively.

Targets	Ti ion		V ion		Cr ion	
	$\overline{E}$	dE/dx	$\overline{E}$	dE/dx	$\overline{E}$	dE/dx
Ge	416	12.1 ± 0.2	474	14.9 ± 0.8	309	11.3 ± 0.6
	387	12.0 ± 0.2	420	17.8 ± 0.7	291	9.0 ± 0.6
	323	11.0 ± 0.3	368	16.6 ± 0.7	240	9.3 ± 0.6
	298	9.9 ± 0.2	223	8.4 ± 0.7	221	9.1 ± 0.6
	281	10.0 ± 0.2	213	8.8 ± 0.7	192	8.5 ± 0.6
	251	10.0 ± 0.2	186	8.1 ± 0.7	173	7.3 ± 0.6
	220	9.7 ± 0.2	168	8.2 ± 0.7	162	6.8 ± 0.5
	194	8.6 ± 0.3			156	7.5 ± 0.6
	184	9.0 ± 0.2			143	6.2 ± 0.5
	170	7.8 ± 0.2				
	162	8.1 ± 0.2				
Au	378	5.4 ± 0.3	455	6.1 ± 0.3	310	5.4 ± 0.3
	273	5.2 ± 0.2	403	6.7 ± 0.2	303	5.9 ± 0.3
	188	4.3 ± 0.2	354	5.5 ± 0.2	287	5.2 ± 0.3
	165	3.7 ± 0.2	202	3.7 ± 0.2	239	4.8 ± 0.3
			177	3.2 ± 0.2	212	4.3 ± 0.3
			160	3.1 ± 0.2	188	4.0 ± 0.3
					164	3.5 ± 0.3
					152	3.2 ± 0.3
					148	3.1 ± 0.3
					134	3.0 ± 0.2

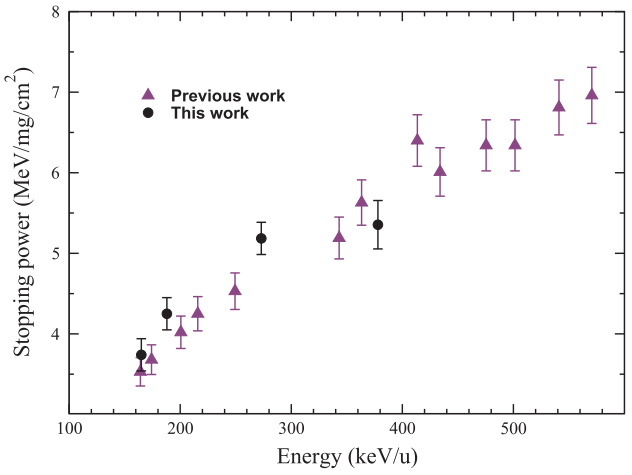

Fig. 4. Comparison between the present and previous [23] experimental data for the electronic stopping power of Ti in Au.

For heavy-ion projectiles, effects such as excitation/ionization [24,25] and electronic screening [1,25] become important with increasing Z (atomic number). These effects are suppressed for proton projectiles and the ESP heavily reflects the electronic structure of the medium. A formal treatment of the atomic collision for heavy ion systems is challenging and it is yet not clear how to disentangle projectile and target atomic features from the ESP.

Among the stopping power theories applied to heavy ion systems, the Unitary Convolution Approximation (UCA) and the Binary theory are two successful ones. The former is a semiclassical theory based on the Bloch theory using an impact-parameter formalism. The energy loss is calculated from a convolution of the electronic density integrated along the ion path [19]. The model has been implemented in the CasP code [26] and allows for some high-order effects, such as projectile screening, projectile excitation and ionization. In our calculations we have set the following physical inputs: mean charge state for projectile screening [27], Barkas binary on and shell corrections on. Shell corrections are relevant at low energies and extend down to 20 keV/u the range of validity of the UCA results. Another significant process in the

stopping power is the contribution due to projectile ionization and excitation. In the CasP code, we considered the ionizations of the projectile and the target by performing independent calculations (for each case). In this case, possible couplings between these two mechanisms are not considered. The total stopping power is given by the sum of these two terms.

The Binary Theory (BT) is based on the Bohr theory but considering the effect of electron binding as a screening to the interaction. In this way, the BT avoids using a perturbation treatment and a distinction between close and distant collisions. In this framework, the Barkas-Andersen effect [28,29] is inherent and shell corrections are duly incorporated.

3.2. Semi-empirical models: The SRIM code and the Northcliffe & Schilling tables

Ziegler, Biersack and Littmark developed a semi-empirical model for the stopping of ions with $Z \leq 92$ over a wide range of energies (from 1 keV/u up to 2 GeV/u) [9]. The stopping of heavy ions for energies higher than 25 keV/u is based on a proper parametrization of the velocity-dependent charge state of the projectile. The model is implemented in the SRIM code and its database is continuously updated.

The Northcliffe and Schilling tables (NS) were developed in the 70's and are often used. It is based on an interpolation/extrapolation procedure, with the available experimental data at that time, to build a series of tables for the stopping power of ions with $1 \leqslant Z \leq 103$ in 24 elements in the 12.5 keV/u–12 MeV/u energy range [8]. The cornerstone of the NS tables is the assumption that the scaling for the stopping of two different materials depends on the projectile's velocity and not on the projectile's atomic number. Aluminum was adopted as the reference material to perform interpolations with the available experimental data and to extrapolate to other projectile-target combinations.

3.3. Comparisons

In Fig. 5 our experimental data are compared with the UCA and BT theories. The UCA theory tends to predict a lower ESP compared to the BT for the projectile-atom combinations explored in this work. The experimental data for Ge agree with the BT while the UCA better describes the data for Au. Both theories underestimate the ESP for V in Ge at energies higher than 300 keV/u. In the light of this comparison solely, the discrepancy observed in both theories might be related to two aspects. The first is the intrinsic differences in the electronic structure of Ge and Au, due to the presence of a small energy band-gap in the former. The second is related to the accurate description of the projectile excitation as an energy loss mechanism. It is expected that projectile excitation is not a dominant process for heavy target atoms (Au in this work) for instance. This subject requires a systematic analysis of many experimental data for a complete picture.

A comparison of our experimental data with the SRIM code (version 2013) and the NS tables is shown in Fig. 5 for Ge and Au targets. The SRIM code describes reasonably well the ESP for Ti projectiles in Ge and Au but overestimates it for Cr projectiles. On the other hand, the NS tables underestimate the stopping power of Ti ions in Ge and Au while exhibiting a good agreement for Cr ions. For V, both semi-empirical models underestimate the stopping power in Ge for energies between 350 keV/u and 500 keV/u even though a better agreement is achieved at lower energies.

3.4. Velocity-proportional dependence

Theoretical models based on linear response theory or density function theory (DFT) reveal that the ESP is proportional to the projectile velocity [15]. The stopping power of protons and deuterium in Al is a textbook example of this velocity dependence.

On the other hand, the stopping in semiconductor and insulator materials exhibit a different behavior. For such materials, the excitation of electron–hole pairs between the valence and conduction bands is important. Only valence electrons contribute to ESP, which is responsible for the appearance of a velocity threshold (v_{th}). For instance, for Ge, the band gap is about $E_{gap} \approx 0.67$ eV (at room temperature) and experimental data for the ESP of protons in Ge shows that $v_{th} = 0.0274$ a. u. [13]. In LiF, a insulator with $E_{gap} \approx 14$ eV, has a $v_{th} \approx 0.1$ eV [30]. From these experimental observations there are indications that the presence of a band-gap in the electronic structure of the target material suppresses the ESP a low velocities.

In noble metals, like Cu and Au, the ESP exhibits a deviation of the slope that is related to the contribution of the d-electrons in the atomic collision. At velocities below the velocity threshold (v_{th}), the ESP is null. For Cu and Au, the $v_{th} \approx 0.18$ a. u. [11,12] and below this velocity, the stopping is determined by the nuclear collisions only.

The relationship between v_{th} and the E_{gap} of the materials is not so straightforward. Besides, the electronic structure of heavy ion projectiles can blur the effects due to the target material. Fig. 6 shows the ESP of Ti, V and Cr in Ge and Au as a function of the projectile velocities (in atomic units). The experimental uncertainties of the data points

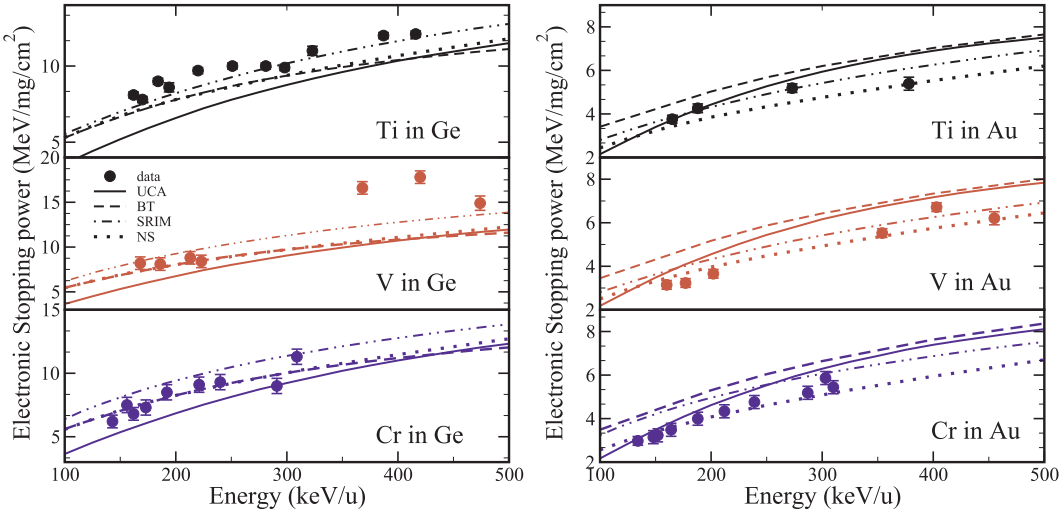

Fig. 5. Comparisons between experimental data and predictions from: i) the Unitary Convolution Approximation (UCA, continuous lines), ii) the Binary Theory (BT, dashed lines), iii) the SRIM code (dotter dashed lines) and iv) the Northcliffe and Schilling tables (NS, dotted lines) for Ti, V and Cr ions slowing down in Ge (left) and Au (right). The difference between the NS and the BT curves is almost imperceptible for the electronic stopping power in Ge.

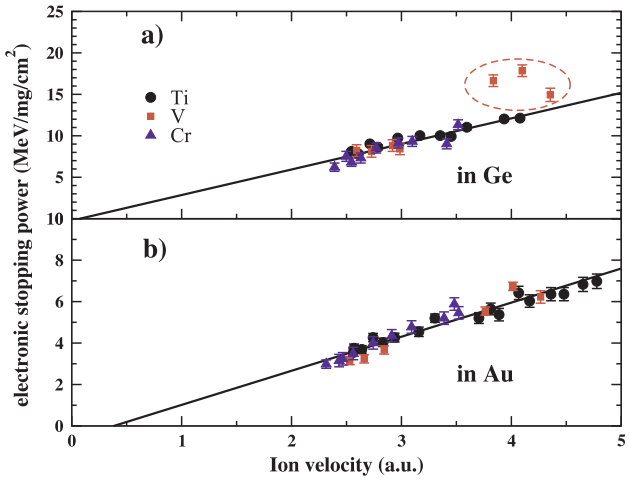

Fig. 6. Velocity dependence of the ESP for Ti, V and Cr projectiles in Ge (panel a) and Au (panel b). Selected data points for V in Ge (indicated by the dashed red ellipsis) have been not considered in the linear regresion. (For interpretation of the references to colour in this figure legend, the reader is referred to the web version of this article.)

allow us to perform a single linear fit for all three projectiles. In Ge (panel a), if we disregard the three highest velocities for V, a good linear dependence is observed as well as in Au (panel b). This is an indication that the electronic structure of the target atom is the main physical input to describe the ESP for these projectiles. Based on a simple linear extrapolation of the experimental data towards low velocities, we point out that the possible v_{th} in Ge is quite small compared to the Au. Present experimental data does not allow an accurate evaluation of this discrepancy. Moreover one can not rule out a possible pronounced kink in the slope for Au as observed in the ESP of the proton in Cu [12].

4. Conclusions

In this paper we present new experimental data for the energy loss of Ti, V and Cr in Ge and Au. Independent measurements of Ti in Au agree with our previous data [23], showing the reproducibility of our experimental technique. We have compared the new data with the UCA, BT, SRIM models and the NS tables. An overall good agreement of the BT is observed for electronic stopping power in Ge despite a small deviation for Ti projectiles. The UCA agrees quite well with ESP for Ti and Cr in Au at energies below ~250 keV/u. The SRIM code overestimates the electronic stopping power for V and Cr which indicates a need for more experimental data for ions for the atomic mass ~50 a.m.u.. The present experimental data point to a velocity-proportional dependence of the ESP even at velocities higher than $v = 1$ a. u.. The extrapolation of the ESP towards low velocities indicates a lower v_{th} for Ge than Au, as observed in experimental data with proton projectiles. The effect of the electronic structure of heavy ions in the stopping power at low velocities still requires more experimental data.

Acknowledgements

R.L. and C.C.S. would like to acknowledge financial support received from the Fundação de Amparo à Pesquisa do Estado do Rio de Janeiro (FAPERJ). R.V.R., N.H.M., J.R.B.O., would like to acknowledge financial support received from the Conselho Nacional de Desenvolvimento Científico e Tecnológico (CNPq). R.L. kindly thanks P. Sigmund for providing us the calculations within the Binary Theory.

References

[1] P. Sigmund, Particle Penetration and Radiation Effects: General Aspects and Stopping of Swift Point Charges, Springer Series in Solid-State Science Vol. 1 Springer-Verlag, Germany, 2006, p. 437.
[2] K. Arstila, J. Keinonen, P. Tikkanen, A. Kuronen, Phys. Rev. B 43 (1991) 13967.
[3] J. Keinonen, K. Arstila, P. Tikkanen, Appl. Phys. Lett. 60 (1992) 228, http://dx.doi.org/10.1063/1.106972.
[4] F. Brandolini, N. Medina, M.D. Poli, P. Pavan, M. Wilhelm, A. Dewald, G. Pascovici, Nucl. Instrum. Methods Phys. Res., Sect. B 132 (1997) 11.
[5] F. Brandolini, R. Ribas, Nucl. Instrum. Methods Phys. Res., Sect. A 417 (1998) 150.
[6] P. Sigmund, Phys. Rev. A 54 (3113) (1996).
[7] U. Fano, Annu. Rev. Nucl. Sci. 13 (1963) 1.
[8] L.C. Northcliffe, R.F. Schilling, Nucl. Data Tables A7 (1970) 233.
[9] J.F. Ziegler, J.P. Biersack, U. Littmark, The Stopping and Ranges of Ions in Matter, first ed., Ziegler-85, 1985, Pergamon Press.
[10] J. Lindhard, M. Scharff, Phys. Rev. 124 (1961) 128.
[11] J.E. Valdés, J.C. Eckardt, G.H. Lantschner, N.R. Arista, Phys. Rev. A 49 (1994) 1083.
[12] S.N. Markin, D. Primetzhofer, M. Spitz, P. Bauer, Phys. Rev. B 80 (2009) 205105.
[13] D. Roth, D. Goebl, D. Primetzhofer, P. Bauer, Nucl. Instrum. Methods Phys. Res., Sect. B 317 (61) (2013) 16–21.
[14] A.A. Correa, J. Kohanoff, E. Artacho, D. Sánchez-Portal, A. Caro, Phys. Rev. Lett. 108 (2012) 213201.
[15] P.M. Echenique, R.M. Nieminen, J.C. Ashley, R.H. Ritchie, Phys. Rev. A 33 (1986) 897.
[16] R. Linares, J.A. Freire, R.V. Ribas, N.H. Medina, J.R.B. Oliveira, E.W. Cybulska, W.A. Seale, N. Added, M.A.G. Silveira, K.T. Wiedemann, Nucl. Instrum. Methods Phys. Res., Sect. B 263 (2007) 345.
[17] P. Petkov, A. Dewald, P. von Brentano, Nucl. Instrum. Methods Phys. Res., Sect. B 560 (2006) 564.
[18] G. Schiwietz, P.L. Grande, Nucl. Instrum. Methods Phys. Res., Sect. B 153 (1999) 1.
[19] P.L. Grande, G. Schiwietz, Nucl. Instrum. Methods Phys. Res., Sect. B 195 (2002) 55.
[20] P. Sigmund, A. Schinner, Nucl. Instrum. Methods Phys. Res., Sect. B 195 (2002) 64.
[21] J.F. Ziegler,www.srim.org/, accessed February 4, 2017.
[22] R.V. Ribas, N.H. Medina, N. Added, J.R.B. Oliveira, E.W. Cybulska, M.N. Rao, W.A. Seale, F. Brandolini, M.A. Rizzutto, J.A. Alcántara-Nunez, Nucl. Instrum. Methods Phys. Res., Sect. B 211 (2003) 453.
[23] R. Linares, J.A. Freire, R.V. Ribas, N.H. Medina, J.R.B. Oliveira, AIP Conf. Proc. 1139 (162) (2009).
[24] S. Damache, S. Ouichaoui, D. Moussa, A. Dib, Nucl. Instrum. Methods Phys. Res., Sect. B 249 (2006) 22.
[25] P. Sigmund, G. Höhler (Ed.), Spinger tracts in modern physics, Vol. 204 Springer, 2004, p. 157.
[26] G. Schiwietz, P.L. Grande,http://www.casp-program.org/, accessed November 20, 2016.
[27] G. Schiwietz, P.L. Grande, Nucl. Instrum. Methods Phys. Res., Sect. B 175–177 (2001) 125.
[28] W.H. Barkas, J.N. Dyer, H.H. Heckman, Phys. Rev. Lett. 11 (1963) 26.
[29] H. Andersen, H. Simonsen, H. Srensen, Nucl. Phys. A 125 (1969) 171.
[30] M. Draxler, S.P. Chenakin, S.N. Markin, P. Bauer, Phys. Rev. Lett. 113201 (2005).